

Tyrosyltyrosylcysteine-Directed Synthesis of Chiral Cobalt Oxide Nanoparticles and Peptide Conformation Analysis

Hyeho Kim,[#] Kyeong-Mi Bang,[#] Heonjin Ha, Nam Heon Cho, Seok Daniel Namgung, Sang Won Im, Kang Hee Cho, Ryeong Myeong Kim, Won Il Choi, Yae-Chan Lim, Ji-Yeon Shin, Hyun Kyu Song, Nak-Kyo Kim,* and Ki Tae Nam*



Cite This: *ACS Nano* 2021, 15, 979–988



Read Online

ACCESS |

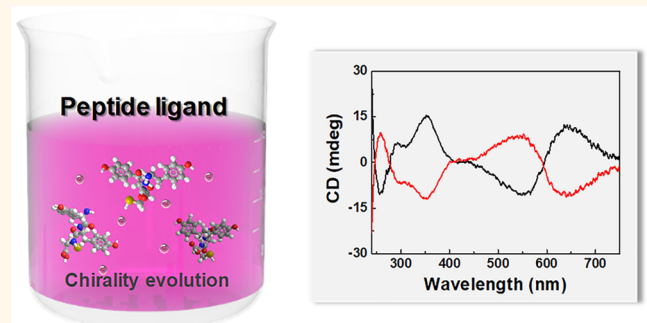
Metrics & More

Article Recommendations

Supporting Information

ABSTRACT: Chiral inorganic nanomaterials have revealed opportunities in various fields owing to their strong light-matter interactions. In particular, chiral metal oxide nanomaterials that can control light and biochemical reactions have been highlighted due to their catalytic activity and biocompatibility. In this study, we present the synthesis of chiral cobalt oxide nanoparticles with a *g*-factor of 0.01 in the UV-visible region using L- and D-Tyr-Tyr-Cys ligands. The conformation of the Tyr-Tyr-Cys peptide on the nanoparticle surfaces was identified by 2D NMR spectroscopy analysis. In addition, the sequence effect of Tyr-Tyr-Cys developing chiral nanoparticles was analyzed. The revealed peptide structure, along with the experimental results, demonstrate the important role of the thiol group and carboxyl group of the Tyr-Tyr-Cys ligand in chirality evolution. Importantly, due to the magnetic properties of chiral cobalt oxide nanoparticles and their strong absorption in the UV region, the circular dichroism (CD) responses can be dramatically modulated under an external magnetic field.

KEYWORDS: chirality, cobalt oxide nanoparticle, Tyr-Tyr-Cys, peptide ligand, magnetic circular dichroism, NMR



Chiral inorganic nanomaterials have been in the limelight of a fundamental understanding of the relationship between chirality and physical properties since the discovery of the different rotations of linearly polarized light in quartz crystals in 1811.¹ Due to the strong light-matter interaction, there has been an increasing demand for chiral inorganic nanomaterials in various fields such as optics, biosensing, and displays. In recent years, the development of such chiral inorganic nanomaterials has been expanding to the realization of exceptional abilities to manipulate light with a negative refractive index,^{2,3} holographic displays,^{4,5} and control of the angular momentum of light.^{6–8} Although the fundamental studies and technological fabrication of chiral nanomaterials have been mainly focused on metals, chiral metal oxide nanomaterials that can control the light and biochemical reactions have triggered huge interest owing to their applicabilities.^{9–12} Considering the catalytic activity and biocompatibility,¹³ development of chiral metal oxide nanomaterials could reveal versatile applications for biomimetic catalysts and medical devices.

Over the past two decades, controllable and scalable methods of synthesizing chiral inorganic nanoparticles have been actively pursued using biomolecules including amino acids,^{14–18} peptides,^{19–21} and DNA.^{22–25} In biological systems, chiral structures develop utilizing chirality transfer from molecules to crystals, and beautiful examples of this can be found in snails, gastropods, and butterfly wings.^{26,27} By mimicking the chirality transfer of nature, various nanomaterials such as chiral gold clusters,²⁸ CdS,²⁹ CdTe,³⁰ ZnO,¹⁴ and Co₃O₄¹⁰ have been developed using peptides and biomolecules, typically cysteine and glutathione. These nanocrystals with a chirally distorted lattice exhibited a chiroptical signal even in the visible light range. Recently, we developed a synthesis

Received: September 11, 2020

Accepted: December 10, 2020

Published: December 17, 2020



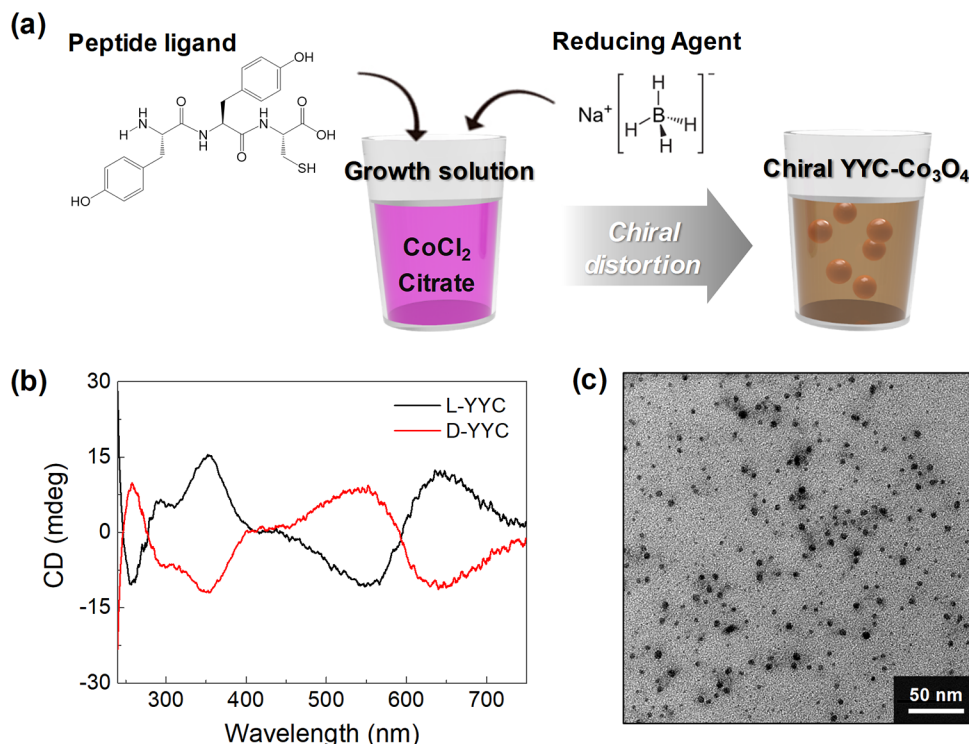


Figure 1. Synthesis of chiral cobalt oxide nanoparticles using Tyr-Tyr-Cys. (a) Illustration of a solution-based method for developing chiral cobalt oxide nanoparticles using a peptide ligand and reducing agent. Tyr-Tyr-Cys was injected into the growth solution as a chiral ligand. (b) Circular dichroism spectra of L- (black line) and D-Tyr-Tyr-Cys-directed nanoparticles (red line). The nanoparticles synthesized using enantiomers showed mirror-symmetric CD responses. (c) TEM image of synthesized chiral cobalt oxide nanoparticles. Scale bar is 50 nm.

platform for chiral gold nanoparticles using cysteine and cysteine-containing peptides that strongly interact with inorganic surfaces.^{31–33} Utilizing the enantioselective interaction of the peptides, synthesized nanoparticles showed mirror-imaged structural chirality and resulting chiroptical responses according to the handedness of the chiral ligand used during synthesis.

To understand and design the mechanism by which the peptide evolves chirality in nanocrystals, it is important to understand the binding and configuration of the peptide on the crystal surface. The exceptional ability of peptides that interact with inorganic surfaces results in the reconstruction of local atomic conformation and evolves a macroscopic chiral structure.³⁴ The functional groups of peptides, including amine groups, thiol groups, and carboxylic groups, interact with the inorganic surface to form strong and weak bonds. These interactions cause local distortion of the inorganic materials to develop a chiral structure, generating chiroptical responses even in the visible light range. Considering the role of the peptide as a chirality inducer, the configuration and binding properties of peptides are highly important in chirality evolution using the peptide–inorganic interaction.^{35,36} In this context, many efforts have been made to analyze the surface state of the ligand using density functional theory (DFT) and molecular dynamics simulation.^{10,11,13} Yeom *et al.* fabricated a chirally distorted Co₃O₄ crystal using L- and D-cysteine molecules and analyzed the circular dichroism (CD) response through a computational study using a model nanoparticle.¹⁰ In addition, Le *et al.* analyzed the orbital couplings between the chiral ligands and cysteine-decorated molybdenum oxide nanoparticles utilizing time-dependent density functional theory (TDDFT) simulation,¹¹ and Jiang *et al.* demonstrated

that the packing of the WO₃ lattice was distorted after L- and D-aspartic acid were adsorbed on the surface through molecular dynamics simulation.¹³ Despite these efforts, experimental and direct evidence showing the configuration of the peptide on the surface is lacking.

Existing studies on chiral metal oxides have focused on the expression of chirality using a single amino acid. However, to understand the mechanism of chirality development and to achieve scalable chiroptical responses, sequence expansion to peptides is an essential step. In this regard, peptides including tyrosine and cysteine, which have received significant attention recently due to their versatile applicability as self-assembled structures and peptide–inorganic hybrid materials,^{37–40} are suitable candidates for the development of chiral functional peptide-based materials. Tyrosine with a phenolic functional group is an important amino acid in controlling the structural conformation of proteins, and its redox-active properties promote charge transport by proton-coupled electron-transfer reactions in natural systems.^{41,42} The thiol side chain in cysteine also serves an important structural role in many proteins.⁴³ Inspired by the fascinating properties of tyrosine and cysteine, our group developed assembling motifs composed of short peptides with tyrosine and cysteine to investigate their structure and potential applications.⁴⁴ The detailed structure of the YYACAYY dimer, which was assembled into macroscopic 2D nanosheets, was revealed by 2D NMR spectroscopy. In the revealed structure, the phenolic groups of tyrosine were facing toward the solvent to form an α -helical secondary structure, and cysteine provided folding stability through disulfide bridges, which are essential for assembly. Based on the tremendous potential of tyrosine and cysteine as structural and functional materials, we believe that a

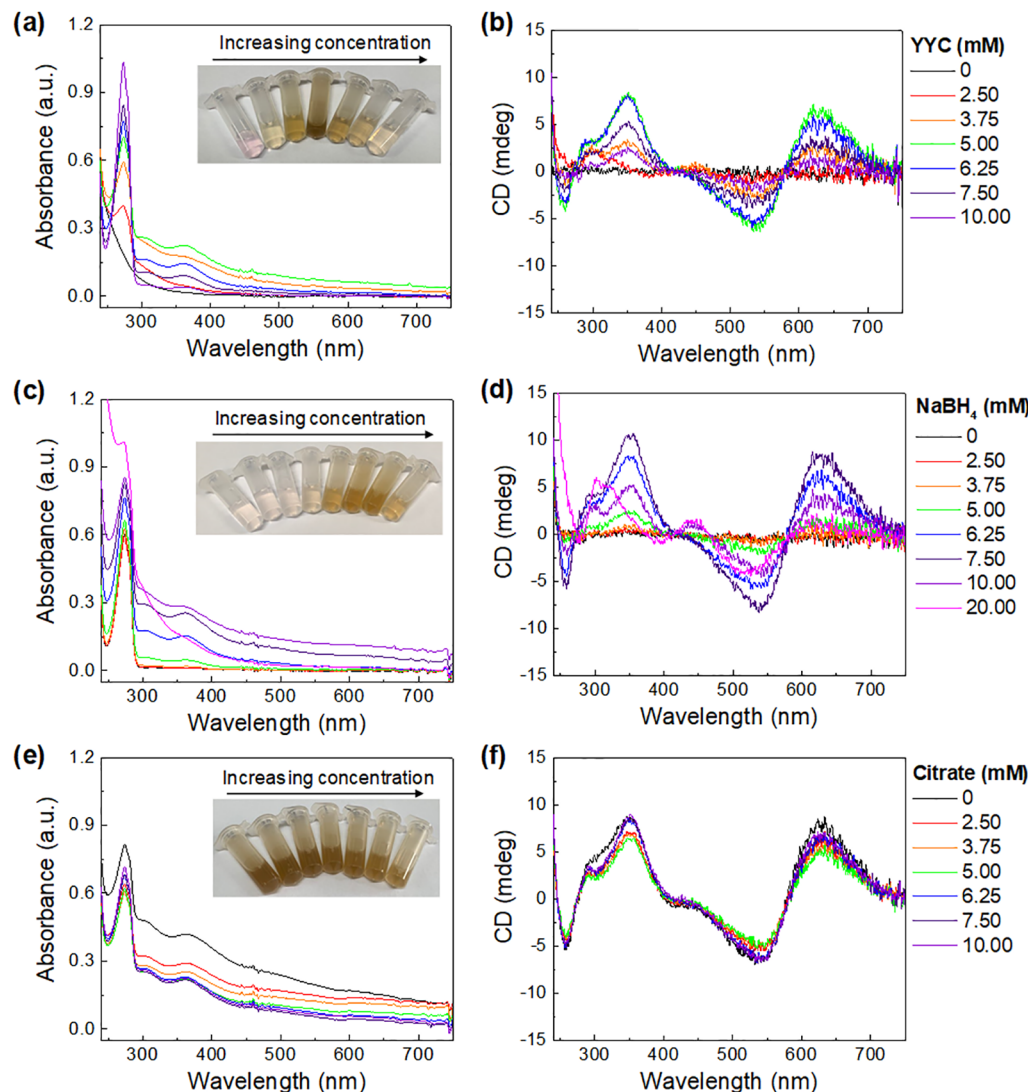


Figure 2. Effect of synthetic parameters on chirality evolution of chiral cobalt oxide nanoparticles. The molar concentrations of Tyr-Tyr-Cys, sodium borohydride (NaBH_4), and citrate were adjusted, while the concentration of cobalt ion in the growth solution was fixed at 5 mM. (a) Absorbance spectra and (b) CD spectra of nanoparticles synthesized using Tyr-Tyr-Cys at various concentrations from 0 to 10 mM. (c) Absorbance spectra and (d) CD spectra of nanoparticles synthesized at various NaBH_4 concentrations from 0 to 20 mM. (e) Absorbance spectra and (f) CD spectra of nanoparticles synthesized at various citrate concentrations from 0 to 10 mM. The images of the synthesized nanoparticle solutions are shown in the inset.

peptide composed of tyrosine and cysteine can be applied to the development of chiral functional peptide-based materials. Furthermore, we intend to discuss the structure of peptides that impart different characteristics to materials through 2D NMR studies.

Here, we report the synthesis of chiral cobalt oxide nanoparticles using a Tyr-Tyr-Cys peptide ligand. The L- and D-Tyr-Tyr-Cys-directed cobalt oxide nanoparticles exhibited mirror-symmetric chiroptic responses with a dis-symmetry factor (*g*-factor) of 0.01 in the UV and visible light regions. Through the control of synthetic parameters of Tyr-Tyr-Cys, citrate, and NaBH_4 , the mechanism of particle formation was analyzed, and the synthetic conditions were optimized. In addition, the 3D structure of the Tyr-Tyr-Cys ligand on the surface of the nanoparticle was determined by 2D NMR. This result indicates that the thiol and carboxylic groups of Tyr-Tyr-Cys were aligned in a single direction and strongly interacted with the nanoparticle surfaces, thereby providing an in-depth

understanding of the configuration and binding of the peptide ligand. Furthermore, the pivotal role of the C-terminal carboxylic group of Tyr-Tyr-Cys to develop nanoparticles was analyzed through sequence effect studies. In addition, the use of peptide ligands of different sequences produced dissimilar chiroptic responses, suggesting the important role of the peptide functional group as well as the scalability of chiral nanomaterial synthesis using peptides. Owing to the intrinsic chirality and magnetic properties of the chiral cobalt oxide nanoparticles, the chiroptic properties, which are considered a permanent feature of the material, could be modulated by an external magnetic field.

RESULTS AND DISCUSSION

Chiral cobalt oxide nanoparticles were synthesized through a solution-based growth method, exploiting the structure-guiding properties of the peptide ligand (Figure 1a). Cobalt chloride, sodium citrate, and Tyr-Tyr-Cys were used as cobalt ion

sources, cobalt ion stabilizers, and chirality inducers, respectively. Possessing cysteine, which provides high-affinity metal binding due to its thiol group, and tyrosine with a redox-active phenolic group that facilitates proton-mediated electron transport, Tyr-Tyr-Cys is a suitable candidate for a peptide ligand. To synthesize chiral cobalt oxide nanoparticles, a growth solution was prepared by mixing cobalt chloride and sodium citrate to stabilize the Co(II) ion. The color of the solution was pink because of the cobalt divalent ion. To encode chirality, Tyr-Tyr-Cys was added to the growth solution and stirred for 30 min. The reaction started with the addition of sodium borohydride (NaBH_4) as the reducing agent. As the reaction proceeded, the pink color of the growth solution gradually turned brown. The reaction was continued for 2 h at room temperature under stirring. The thiol and carboxylic groups of Tyr-Tyr-Cys strongly bind to the cobalt oxide surface to develop nanoparticles. During nanoparticle formation, the interaction between Tyr-Tyr-Cys and the surface chirally distorts the local atomic conformation of the nanoparticle surfaces, generating chirality.

Using the Tyr-Tyr-Cys ligand, chiral cobalt oxide nanoparticles with chiroptical properties were synthesized. The transmission electron microscopy (TEM) image in Figure 1c further confirmed that nanoparticles of about 5 nm in size were synthesized using a peptide ligand. When observed through high-resolution transmission electron microscopy (HRTEM) and Raman analysis, the cobalt oxide is close to the amorphous structures probably due to the surface distortion by the peptide ligand (Figure S1). X-ray photoelectron spectroscopy (XPS) data showed the coexistence of Co(II) and Co(III), and in accordance with XPS, the UV-visible spectrum exhibited typical peaks at 500 and 660 nm, which can be assigned as O(II) → Co(III) transition and Co(III) d-d transition, which are similarly observed in previously reported Co_3O_4 (Figures S1 and S2).^{45,46} Thus, we think that the composition and valency of the synthesized nanoparticles are close to the spinel Co_3O_4 , while the structure is distorted. CD and absorbance spectra of the chiral cobalt oxide nanoparticles were evaluated in the UV-visible region. Chiral cobalt oxide nanoparticles showed clear chiroptical responses with five positive and negative peaks, as shown in Figure 1b. This distinct optical spectrum showed clear differences from previously reported chiral cobalt oxide synthesized using a single amino acid.¹⁰ Nanoparticles synthesized using L- and D-Tyr-Tyr-Cys ligands showed perfect mirror-symmetric CD signal with coincident peak positions and zero crossing points. In detail, CD peaks at 260, 290, and 350 nm in the UV region and peaks at 550 and 640 nm in the visible region originating from ligand to metal charge transfer (LMCT) with a small fraction of intraparticle Co(II) → Co(III) d-d transitions were observed.¹⁰ When converted to Kuhn's dis-symmetry value, g-factor, chiral cobalt oxide nanoparticles showed a maximum g-value of 0.01 at a wavelength of 640 nm (Figure S3). L- and D-Tyr-Tyr-Cys-directed nanoparticles showed almost the same absorbance spectra with a strong absorbance peak at 274 nm and a shoulder at 280 nm from the absorption of the Tyr-Tyr-Cys tyrosine residue with a small fraction of the O(II) → Co(II) transition (Figures S2 and S4).^{47–49} In addition, chiral cobalt oxide nanoparticles had characteristic peaks at 303 and 363 nm by ligand to cobalt charge transfer.^{45,50,51}

To understand the underlying mechanism of chiral nanoparticle formation and optimize the synthesis conditions, the synthesis parameters were controlled during growth. The

molar concentrations of sodium citrate, Tyr-Tyr-Cys peptide ligand, and NaBH_4 were adjusted, while the concentration of cobalt ions in the growth solution was fixed at 5 mM (Figure 2). The Tyr-Tyr-Cys ligand, which imparts chirality to the nanoparticles, plays an important role in nanoparticle formation. In the absence of Tyr-Tyr-Cys, the solution appeared pinkish, indicating that no cobalt oxide nanoparticles were produced (Figure 2a). At 3.75 mM, the growth solution exhibited a light brown color, and above 5 mM, characteristic absorption peaks at 303 and 363 nm of cobalt oxide nanoparticles were observed, indicating that the cobalt oxide nanoparticles were successfully synthesized. The color of the solution became light at higher concentrations, suggesting that the yield of nanoparticles decreased. The CD response increased as the concentration increased, showing the highest value with distinct peaks at 5 mM Tyr-Tyr-Cys (Figure 2b). At higher concentrations, the CD value decreased as the particle yield decreased. The highest g-factor of 0.011 was achieved at a Tyr-Tyr-Cys concentration of 6.25 mM. At higher concentrations, the g-factor was saturated, and the yield was reduced.

The concentration of the reducing agent NaBH_4 also greatly influences the yield and synthesis kinetics of the chiral cobalt oxide nanoparticles. At low concentrations of less than 3.75 mM, particles are hardly formed, resulting in a transparent solution with a CD signal close to zero (Figure 2c,d). As the NaBH_4 concentration increased to 7.5 mM, the particle yield increased and the characteristic absorption peaks of cobalt oxide nanoparticles at 303 and 363 nm appeared and increased. The CD signal in Figure 2d increased with increasing NaBH_4 concentration and produced the highest value at 7.5 mM. At 10 mM NaBH_4 , the yield of the nanoparticles increased but the chirality of the particles decreased. Further increase in concentration largely changed the kinetics for particle formation. Notably, at high NaBH_4 concentrations above 20 mM, the characteristic absorption of cobalt oxide nanoparticles at 303 and 363 nm disappeared and a divergent CD signal was generated, suggesting that nanoparticles with different properties were synthesized.

Citrate is not essential for the formation of nanoparticles, but it modulates the yield and g-factor of the nanoparticles by affecting the reduction of cobalt cations during synthesis. As shown in Figure 2e, the particle solution turned dark brown, showing the characteristic absorption spectrum even at low citrate concentrations. When citrate is in the growth solution, it affects the reduction of cobalt cations, reducing the yield of the nanoparticles. It was observed that as the concentration of citrate increased, the color of the solution changed from dark brown to light brown, and the absorption peaks in the UV-visible region were reduced. The overall shape of the CD spectrum remained similar in the 0–10 mM citrate concentration range (Figure 2f). The CD response decreased slightly as the citrate concentration increased to 5 mM and slightly increased when the concentration was further increased to 10 mM. The chirality index, g-factor, showed the highest value when the citrate concentration was 7.5 mM. Higher concentrations are expected to interfere with particle formation, decreasing the g-value. Taken together, in chiral cobalt oxide nanoparticle synthesis, Tyr-Tyr-Cys peptide and NaBH_4 initiate the synthesis and generate nanoparticles. Citrate affects the reduction of cobalt cations to control the particle yield and g-factor. The optimized synthesis conditions for the highest chiroptical properties with a g-factor above 0.01

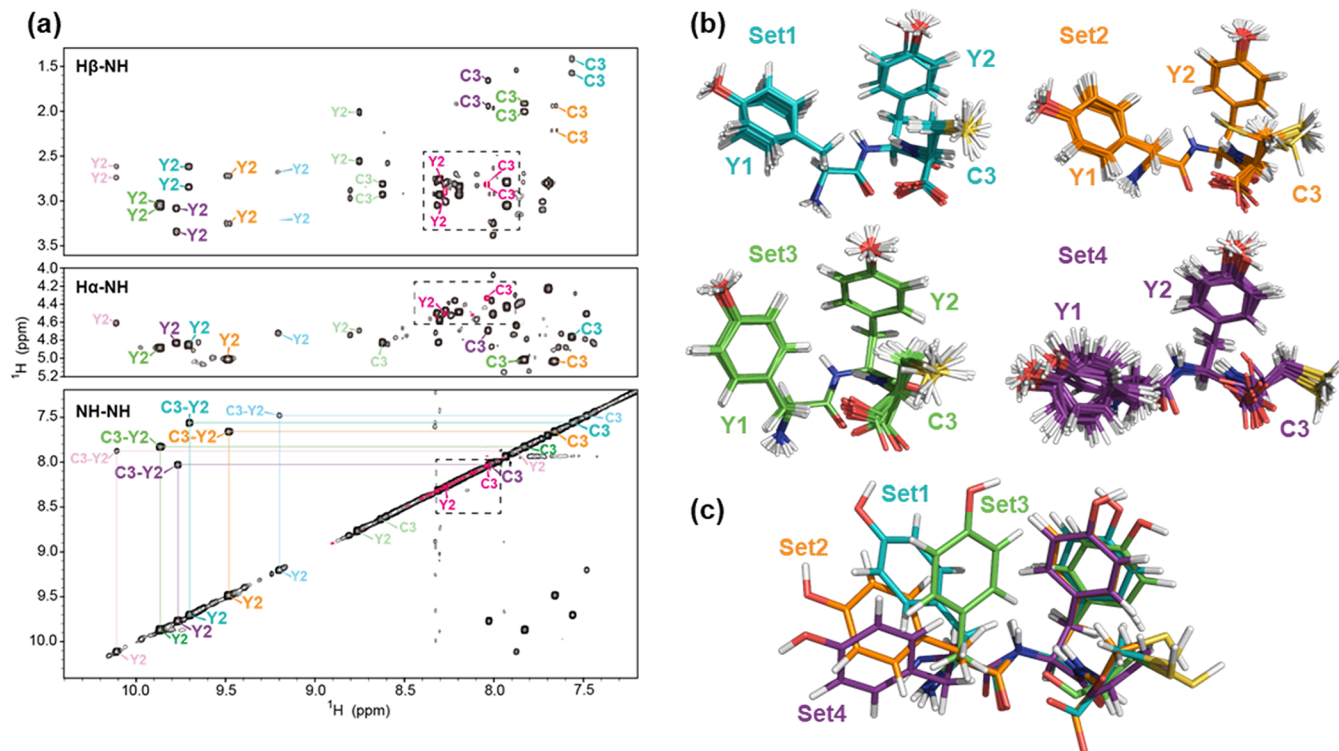


Figure 3. NMR structural analysis of Tyr-Tyr-Cys (Y1-Y2-C3) on chiral cobalt oxide nanoparticles. (a) 2D proton–proton correlation spectra of TOCSY (H α - and H β -NH region) and NOESY (NH-NH region). The NMR spectra of Tyr-Tyr-Cys in the presence (black) and in the absence (magenta in dashed boxes) of cobalt oxide nanoparticle are overlapped. (b) Superimposition of the 20 lowest energy structures of the four representative conformation sets. The assigned resonances in (a) and structures in (b) are colored by each conformation set (set 1: cyan, set 2: orange, set 3: green, and set 4: purple). The colors of the elements C, N, O, H, and S in the structures are green, blue, red, white, and yellow, respectively. (c) Superimposition of the lowest energy structures of each conformation set, which are aligned for the α carbon of backbone.

was found under 5 mM cobalt ion, 7.5 mM citrate, 6.25 mM Tyr-Tyr-Cys, and 6.25 mM NaBH₄ (Figure S5).

The tertiary interaction between Tyr-Tyr-Cys (or Y1-Y2-C3) peptides and cobalt oxide nanoparticles was investigated by NMR analysis. The intact peptides showed only one set of correlation peaks in the H α -NH, H β -NH, and NH-NH regions of the 2D total correlation spectroscopy (TOCSY) and nuclear Overhauser effect spectroscopy (NOESY) spectrum (Figure 3a, magenta in dashed boxes), suggesting that intact peptides have dynamic random structures. However, after treatment with cobalt oxide nanoparticles, the NMR spectra of the peptides showed dramatic changes. First, a large number of new cross-peaks appeared. In addition, at least seven unambiguously distinguishable sets of Tyr-Tyr-Cys cross-peaks were identified (Figure 3a, other colors). Second, the proton resonances showed sizable pseudocontact shifts, which are well known as the changes in chemical shifts due to their close contact with the paramagnetic center, in this case, Co(II).⁵² This observation clearly demonstrated that the peptides directly interacted with cobalt oxide nanoparticles, and as a result, the peptide structures were stabilized, forming several different conformers.

Next, to examine the structural characteristics of Tyr-Tyr-Cys peptides and the binding interaction mode to cobalt oxide nanoparticles, we determined the solution structures of the peptides. Among the more than seven sets of identified Tyr-Tyr-Cys nuclear Overhauser enhancement (NOE) peaks, the four sets that showed a distinct pseudocontact shift with clear NOE peaks were used for 3D structural calculations. The 20

lowest energy structures of all four conformers converged well with a backbone root-mean-square deviation (rmsd) of <0.2 Å (Figure 3b and Table S1). The Y1 of structure 4 was relatively less converged owing to the lack of NOE restraints. Although it is a short peptide composed of Tyr-Tyr-Cys, all four sets of peptides were predicted to have right-handed helical structures based on the distribution of dihedral angles in the Ramachandran plot (Figure S6).⁵³ To determine how Tyr-Tyr-Cys interacts with cobalt oxide nanoparticles, the lowest energy structures of each conformation set were aligned through the α carbon atoms of each residue (Figure 3c). All amide nitrogens and carboxylic oxygens of the backbone as well as the thiol of Cys faced the same direction (Figure 3c). Since cobalt has a great affinity for nitrogen, it is strongly suggested that the tertiary interaction of the peptide with cobalt oxide nanoparticles is through the backbone interface, including the thiol of Cys. The side chains of Y1 and Y2 pointed toward the upper direction, but the directions of the phenol ring of Y1 are different. The angle of the aromatic ring of Tyr1 between sets 3 and 4 was measured to be ~90° (Figure 3c); therefore, we suggest that the slightly different peptide structures might play a role as a building block of cobalt oxide nanoparticles.

Based on our understanding of the configuration of Tyr-Tyr-Cys decorating nanoparticles, the sequence effect was explored to investigate the role of Tyr-Tyr-Cys in developing nanoparticles. First, to explore the role of the N- and C-termini of Tyr-Tyr-Cys in developing chiral nanoparticles, L-Tyr-Tyr-Cys ethyl ester with a blocked carboxylic acid group and N-acetyl-L-

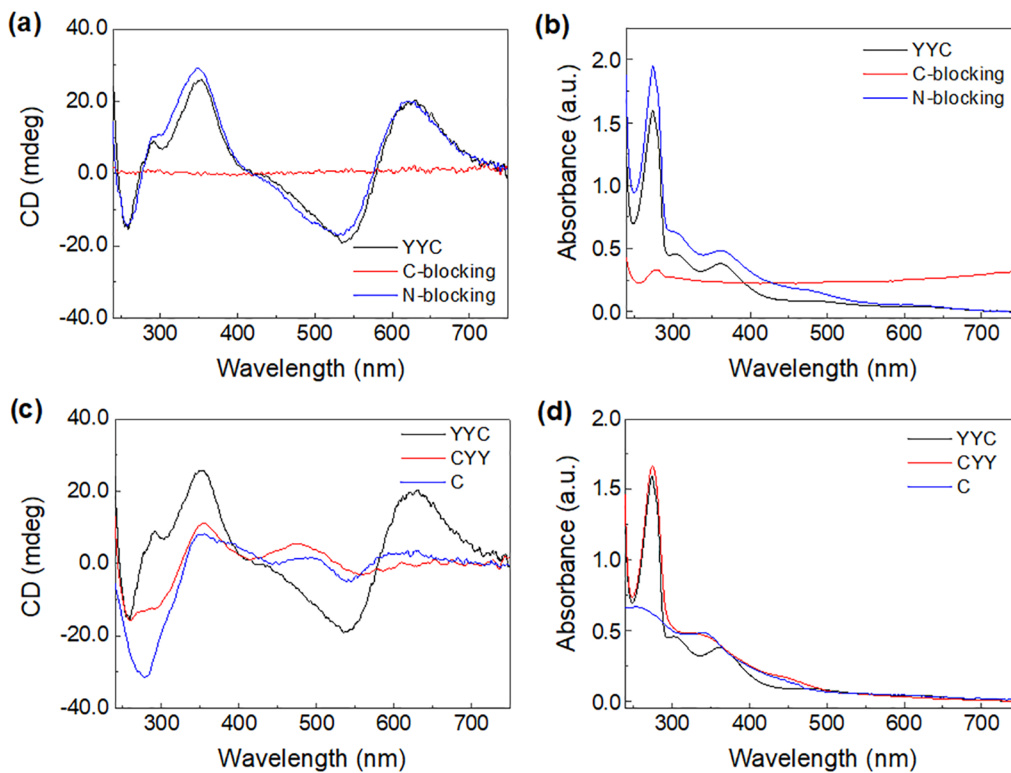


Figure 4. Sequence effect of the Tyr-Tyr-Cys ligand in chiral cobalt oxide nanoparticle evolution. (a) CD spectra and (b) absorbance spectra of the nanoparticles synthesized with Tyr-Tyr-Cys (YYC, black line), C-blocked (red line), and N-blocked Tyr-Tyr-Cys (blue line). For the C- and N-blocking experiments, L-Tyr-Tyr-Cys ethyl ester and N-acetyl-L-Tyr-Tyr-Cys were used for synthesis, respectively. (c) CD spectra and (d) absorbance spectra of nanoparticles synthesized with Tyr-Tyr-Cys (YYC, black line), Cys-Tyr-Tyr (CYY, red line), and cysteine (C, blue line).

Tyr-Tyr-Cys with a blocked amine group were used for synthesis. Along with the NMR data presented above, the terminal blocking experiment suggests that the thiol group and the carboxylic group of Tyr-Tyr-Cys play an important role in chiral nanoparticle evolution (Figure 4). As shown in Figure 4a, blocking the C-terminal of the peptide prevented the formation of the chiral cobalt oxide nanoparticles, resulting in the disappearance of the CD response. The absorbance spectrum of the C-terminal-blocked case showed that the characteristic LMCT peak disappeared due to low nanoparticle yield with a large scattering in the visible–IR region by peptide aggregates (Figure 4b). When the N-terminal of the peptide was blocked, a CD response similar to Tyr-Tyr-Cys-directed nanoparticles was obtained (Figure 4a), while chirality was not observed when the C-terminal was blocked. N-Blocked Tyr-Tyr-Cys-directed nanoparticles showed a similar absorbance spectrum to Tyr-Tyr-Cys-directed nanoparticles, matching the characteristic peaks at 274, 303, and 363 nm (Figure 4b). Detailed observations revealed that the CD peaks in the UV region of the N-blocking coincided with Tyr-Tyr-Cys-directed nanoparticles, but the CD peaks in the visible region were blue-shifted. This result indicates that the N-terminal amine group of Tyr-Tyr-Cys is not dominant in developing chiral nanoparticles, but appears to participate in chirality evolution, altering the CD spectrum.

To provide an in-depth understanding of the role of the Tyr-Tyr-Cys peptide in chiral nanoparticle development, Cys-Tyr-Tyr and cysteine ligands were used for the synthesis and compared to Tyr-Tyr-Cys. Tyr-Tyr-Cys-directed cobalt oxide exhibited a characteristic CD spectrum in the UV–visible

region, as depicted in Figures 1 and 4. However, when Cys-Tyr-Tyr and cysteine were involved as chirality inducers, CD responses different from Tyr-Tyr-Cys were obtained. When Cys-Tyr-Tyr was added instead of Tyr-Tyr-Cys, a CD spectrum with similar peak positions at 260, 290, and 350 nm, but different shapes was obtained in the UV region (Figure 4c). In addition, it exhibited a distinct spectrum with a positive CD peak at 480 nm and a negative peak at 560 nm in the visible region. In the case of cysteine, a continuous spectrum of negative peaks near 290 nm, positive peaks at 350 nm and near 500 nm, and negative peaks near 550 nm were observed, which is considered to be similar to the Cys-Tyr-Tyr case. In addition, nanoparticles synthesized using Cys-Tyr-Tyr and cysteine had distinct absorption spectra from Tyr-Tyr-Cys (Figure 4d). When Cys-Tyr-Tyr was used, a different absorbance spectrum appeared with a peak at 274 nm, with a 280 nm shoulder corresponding to the absorption of tyrosine residues, and a peak at 340 nm originating from LMCT.^{47,50,51} For cysteine-directed nanoparticles, absorption peaks at 260 nm corresponding to the absorption of cysteine and a peak at 340 nm derived from LMCT were observed.⁵⁴ The thiol, amine, and carboxyl groups of the peptide interacted with the inorganic surfaces. Therefore, it is expected that the configuration of the ligand on the interface will be different, depending on the spatial location of the functional groups. We suppose that in the case of cysteine and Cys-Tyr-Tyr, where both amine groups are exposed, thiol and amine groups bind to the NP surface, by order of binding affinity, resulting in different chiroptical properties from Tyr-Tyr-Cys. To further demonstrate the effect of the peptide sequence on the

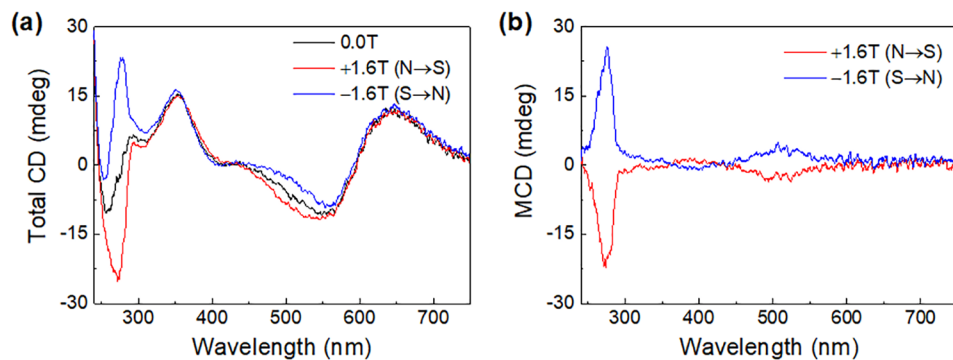


Figure 5. Magnetic circular dichroism (MCD) in chiral cobalt oxide nanoparticles. (a) Total CD spectra and (b) MCD spectra of L-Tyr-Tyr-Cys-directed chiral cobalt oxide nanoparticles. The MCD measurement was conducted under a magnetic field of 1.6 T in the forward (red line) and backward directions (blue line) of the light propagation. The MCD spectrum was obtained by subtracting the natural CD ($B = 0$) from the total CD spectrum.

chiroptical properties of nanoparticles, various cysteine-containing short peptides were demonstrated in the synthesis of chiral cobalt oxide (Figure S7). All of the investigated sequences resulted in different chiroptic responses, which indicates that peptide sequence has a crucial effect on deciding chirality of cobalt oxide nanoparticles.

The chiroptic response of the synthesized cobalt oxide nanoparticles, which are paramagnetic at room temperature, can be modulated by an external magnetic field (Figures 5a and S8a). CD and magnetic circular dichroism (MCD) of chiral cobalt oxide nanoparticles were analyzed according to the presence and direction of a magnetic field and compared with achiral cobalt oxide nanoparticles. Natural CD (NCD), commonly referred to as CD, originates from the different response of the chiral distribution of electric charges toward LCP and RCP light and appears in materials without mirror symmetry. On the other hand, MCD is caused by magnetic field induced Zeeman interaction of electronic structure and is a universal property that arises in any material under a magnetic field.⁵⁵ In chiral materials under a magnetic field, total CD is the sum of NCD, which is dependent upon the chirality of the material, and MCD, which is not, total CD = NCD($B = 0$) + MCD.⁵⁶ Total CD spectra of chiral cobalt oxide nanoparticles synthesized with Tyr-Tyr-Cys were measured in the presence of a magnetic field of 1.6 T in parallel (forward) and antiparallel (backward) directions of light propagation. To evaluate a pure magnetic contribution on circular dichroism, MCD spectra except natural CD obtained without an external magnetic field to total CD are depicted in Figures 5b and S8b. The MCD of the chiral cobalt oxide nanoparticles showed a strong negative peak at a position of the absorption maximum of 274 nm. It also exhibited a relatively small positive peak at 390 nm and a negative peak at 508 nm, which are expected to originate from ligand to cobalt transfer and d-d transition of Co(II) and Co(III), respectively.^{57,58} When the direction of the magnetic field was reversed, the signs of these three peaks were also reversed, showing a symmetrical spectrum.

The strong MCD signal in the UV region of the peptide-directed nanoparticles was achieved by utilizing the absorption of tyrosine residues through peptide–inorganic hybridization. To further analyze this, achiral cobalt oxide nanoparticles were synthesized through a hydrothermal method (Figure S9). MCD spectra of achiral cobalt oxide nanoparticles were measured and compared with chiral cobalt oxide nanoparticles

(Figure S10). Achiral nanoparticles showed broad absorbance peaks from UV to 300 nm corresponding to an O(II) → Co(II) transition and at 340 to 600 nm and around 700 nm, which originated from the O(II) → Co(III) transition (Figure S10a).^{59,60} The achiral nanoparticles did not exhibit a natural CD response in the absence of a magnetic field. When an external magnetic field was applied, it showed broad MCD peaks that were symmetric according to the magnetic field direction due to the intrinsic magnetic properties of cobalt oxide (Figure S10b). Due to the absence of strong absorption of the tyrosine residue in the UV region, the magnitude of the MCD signal was approximately 10 times smaller than that of chiral cobalt oxide nanoparticles, demonstrating that the MCD signal can be improved *via* peptide–inorganic hybridization. Chiral cobalt oxide nanoparticles synthesized using Tyr-Tyr-Cys are optical materials that combine chirality and magnetism and show the versatile potential of chiral nanomaterials for industrial applications by controlling the optical activity that is considered permanent after fabrication or synthesis.

CONCLUSION

In summary, chiral cobalt oxide nanoparticles with a g-factor of 0.01 in the visible range were synthesized using the Tyr-Tyr-Cys ligand. Since chiral nanoparticles were evolved through the interaction between the peptide and the inorganic surfaces, the synthesized nanoparticles exhibited mirror-symmetric chiroptic responses depending on the handedness of the peptides. The role of the chemical parameters that can determine the chirality evolution in the nanoparticles was elucidated, and the synthetic conditions were optimized for a large chiroptic response through experimental demonstration. In the synthesis of chiral cobalt oxide nanoparticles, peptides imparted chirality to nanoparticles and initiated particle formation. NaBH₄ affected the kinetics of particle formation and final yield of the nanoparticles, and citrate adjusted the particle yield and g-factor. In addition, 2D NMR analysis revealed that the thiol and carboxylic groups of the Tyr-Tyr-Cys ligand were aligned in a single direction on the nanoparticle, indicating their strong interaction with the nanoparticle surfaces. Furthermore, the sequence effect of Tyr-Tyr-Cys developing chiral nanoparticles was analyzed. The C-terminal carboxylic group of the peptide exhibited a dominant effect on the chirality expression of the nanoparticles. The use of Cys-Tyr-Tyr and cysteine instead of Tyr-Tyr-Cys generated different chiroptic responses, which are expected to be the effect of exposed amine groups. Given the

diversity of peptides, this suggests the infinite expandability of the synthesis method utilizing peptide ligands. Due to the magnetic properties of chiral cobalt oxide nanoparticles, the chiroptic properties could be modulated by an external magnetic field. The MCD measurements demonstrated that the CD response in the UV and visible regions of the nanoparticles dramatically changed under a magnetic field of 1.6 T. Tyr-Tyr-Cys-directed chiral cobalt oxide nanoparticles exhibit chiroptic properties that can be controlled by an external magnetic field, which is not only important for fundamental studies on spintronics and magneto-optics but can also be widely applied in optoelectronic devices and active displays. Furthermore, chiral cobalt oxide is a peptide-inorganic hybrid metamaterial that combines the redox activity properties of a peptide and the catalytic properties of a metal oxide and is expected to be applied as a proton conductor, an antenna for photoluminescence, and a chiral catalyst.

EXPERIMENTAL METHODS

Chemicals. All peptides (98%) were purchased from BeadTech Inc. (Korea) and used without further purification. Cobalt(II) chloride hexahydrate (97%) was purchased from Junsei (Japan). Sodium citrate tribasic dehydrate (99%) and sodium borohydride (NaBH_4 , 98%) were purchased from Sigma-Aldrich. All aqueous solutions were prepared using high-purity deionized water (DI) (18.2 $\Omega\text{ cm}^{-1}$).

Synthesis of Chiral Cobalt Oxide Nanoparticles. Chiral cobalt oxide nanoparticles were synthesized using a solution-based growth method. For typical synthesis, 0.5 mL of 0.1 M cobalt(II) chloride, 0.75 mL of 0.1 M sodium citrate, and 6.25 mL of a 0.01 M Tyr-Tyr-Cys aqueous solution were added to 1.875 mL of DI. After stirring at room temperature (RT) for 30 min, 0.625 mL of 0.1 M NaBH_4 was injected, followed by aging under stirring for 2 h at RT. The synthesized nanoparticles were analyzed after dialysis using a 1 kDa MWCO membrane.

Synthesis of Achiral Cobalt Oxide Nanoparticles. Achiral cobalt oxide nanoparticles were synthesized using a hydrothermal method. Cobalt(II) acetate tetrahydrate (1 g) was dissolved in 50 mL of ethanol under stirring at 45 °C for 10 min, followed by dropwise addition of 6.6 mL of ammonia solution (25%). The mixture was transferred into a Teflon-lined autoclave and maintained at 150 °C for 3 h. After synthesis, the crude solution was mixed with 200 mL of acetone and centrifuged twice at 135 000 rpm for 20 min. The final product of the nanoparticles was dispersed in DI water for further analysis.

Characterization. Circular dichroism and absorbance spectra of chiral cobalt oxide nanoparticles were obtained using a J-815 spectropolarimeter instrument (JASCO). Kuhn's dis-symmetry factor (g-factor) was calculated from the measured CD value and extinction using the following equation:

$$\text{g-factor} = 2 \frac{A_L - A_R}{A_L + A_R}$$

Magnetic circular dichroism spectra were measured with a J-815 spectropolarimeter instrument (JASCO) equipped with a 1.6 T (tesla) permanent magnet using both the parallel and antiparallel fields. HRTEM images were acquired using a JEM-2100F system (JEOL, Tokyo, Japan) and a Cs-corrected monochromated TEM (Themis Z, Thermo Fisher). The HRTEM images were taken under the acceleration voltage of 200 kV. Raman spectra of cobalt oxide nanoparticles were recorded by a Raman spectrometer (LabRAM HR Evolution, Horiba) using a 50× long working distance visible objective. The wavenumber of the excitation light source was 532 nm. XPS spectra of cobalt oxide nanoparticles were carried out by a photoelectron spectrometer (K-alpha+, ThermoFisher Scientific) with a pass energy of 40 eV.

NMR Spectroscopy. NMR spectra were collected at 298 K on a Bruker Avance III HD 800 MHz spectrometer equipped with a *z*-gradient triple-resonance cryoprobe. The NMR samples were prepared in DI water with 10% (v/v) D_2O . NMR data were processed using the TopSpin3.5pl7 (Bruker) program and analyzed using the NMRFAM-SPARKY program.⁶¹ Two-dimensional TOCSY and NOESY correlation experiments were used to assign the amide, alpha, and beta protons of the Tyr-Tyr-Cys peptides. Interproton distance restraints were obtained from the NOE spectra, and the classified distance ranges by the NOE peak intensities were used for structure calculation. The structures were calculated by simulated annealing using the program CYANA 3.0.⁶² The final 20 lowest-energy structures were visualized using PyMOL (Schrodinger, LLC).

ASSOCIATED CONTENT

SI Supporting Information

The Supporting Information is available free of charge at <https://pubs.acs.org/doi/10.1021/acsnano.0c07655>.

Chiral cobalt oxide characterization; absorbance spectrum of the nanoparticles synthesized with L- and D-Tyr-Tyr-Cys; g-factor spectrum of the nanoparticles synthesized with L- and D-Tyr-Tyr-Cys; CD and absorbance spectra of L- and D-YYC peptide solution; effect of synthetic parameters on g-factor of chiral cobalt oxide nanoparticles; backbone dihedral angles (φ and ψ) of the peptides on chiral cobalt nanoparticles; synthesis of chiral cobalt oxide nanoparticles using various peptides; total CD spectra and MCD spectra of D-Tyr-Tyr-Cys-directed chiral cobalt oxide nanoparticles; achiral cobalt oxide characterization; absorbance and MCD spectra spectrum of achiral cobalt oxide nanoparticles; structural statistics for the final 20 structures of four representative conformation sets of the Tyr-Tyr-Cys peptide on chiral cobalt oxide nanoparticles (PDF)

AUTHOR INFORMATION

Corresponding Authors

Nak-Kyo Kim – Advanced Analysis Center, Korea Institute of Science and Technology, Seoul 02792, Republic of Korea; Email: nkkim@kist.re.kr

Ki Tae Nam – Department of Materials Science and Engineering, Seoul National University, Seoul 08826, Republic of Korea; orcid.org/0000-0001-6353-8877; Email: nkitae@snu.ac.kr

Authors

Hyeohn Kim – Department of Materials Science and Engineering, Seoul National University, Seoul 08826, Republic of Korea

Kyeong-Mi Bang – Department of Life Sciences, Korea University, Seoul 02841, Republic of Korea; Advanced Analysis Center, Korea Institute of Science and Technology, Seoul 02792, Republic of Korea

Heonjin Ha – Department of Materials Science and Engineering, Seoul National University, Seoul 08826, Republic of Korea

Nam Heon Cho – Department of Materials Science and Engineering, Seoul National University, Seoul 08826, Republic of Korea

Seok Daniel Namgung – Department of Materials Science and Engineering, Seoul National University, Seoul 08826, Republic of Korea

Sang Won Im – Department of Materials Science and Engineering, Seoul National University, Seoul 08826, Republic of Korea
Kang Hee Cho – Department of Materials Science and Engineering, Seoul National University, Seoul 08826, Republic of Korea
Ryeong Myeong Kim – Department of Materials Science and Engineering, Seoul National University, Seoul 08826, Republic of Korea
Won Il Choi – Department of Materials Science and Engineering, Seoul National University, Seoul 08826, Republic of Korea
Yae-Chan Lim – Department of Materials Science and Engineering, Seoul National University, Seoul 08826, Republic of Korea
Ji-Yeon Shin – Department of Life Sciences, Korea University, Seoul 02841, Republic of Korea; Advanced Analysis Center, Korea Institute of Science and Technology, Seoul 02792, Republic of Korea
Hyun Kyu Song – Department of Life Sciences, Korea University, Seoul 02841, Republic of Korea;  orcid.org/0000-0001-5684-4059

Complete contact information is available at:
<https://pubs.acs.org/10.1021/acsnano.0c07655>

Author Contributions

#H. Kim and K.-M. Bang contributed equally to this work.

Notes

The authors declare no competing financial interest.

ACKNOWLEDGMENTS

This research was supported by Creative Materials Discovery Program through the National Research Foundation of Korea (NRF) funded by Ministry of Science and ICT (NRF-2017M3D1A1039377), the KIST-SNU Joint Research Lab project (2 V06170) under the KIST Institutional Program funded by the Korean government (Ministry of Science, ICT & Future Planning), and the National Research Foundation of Korea (NRF) grant funded by the Korean government (MSIT) (NRF-2017R1A2B3012003). This work was supported by LG Display under the LGD-SNU Incubation Program. K.T.N. appreciates the support from Institute of Engineering Research, Research Institute of Advanced Materials (RIAM), and Soft Foundry at Seoul National University.

REFERENCES

- (1) Arago, F. J. D. *Memoires de La Classe Des Sciences Mathematiques et Physiques de l'Institut Imperial de France*; Didot: Paris, France, 1811.
- (2) Pendry, J. B. A Chiral Route to Negative Refraction. *Science* **2004**, *306*, 1353–1355.
- (3) Zhang, S.; Park, Y.-S.; Li, J.; Lu, X.; Zhang, W.; Zhang, X. Negative Refractive Index in Chiral Metamaterials. *Phys. Rev. Lett.* **2009**, *102*, 023901.
- (4) Wen, D.; Yue, F.; Li, G.; Zheng, G.; Chan, K.; Chen, S.; Chen, M.; Li, K. F.; Wong, P. W. H.; Cheah, K. W.; Yue Bun Pun, E.; Zhang, S.; Chen, X. Helicity Multiplexed Broadband Metasurface Holograms. *Nat. Commun.* **2015**, *6*, 8241.
- (5) Khorasaninejad, M.; Ambrosio, A.; Kanhaiya, P.; Capasso, F. Broadband and Chiral Binary Dielectric Meta-Holograms. *Sci. Adv.* **2016**, *2*, No. e1501258.
- (6) Schäferling, M.; Yin, X.; Engheta, N.; Giessen, H. Helical Plasmonic Nanostructures as Prototypical Chiral Near-Field Sources. *ACS Photonics* **2014**, *1*, 530–537.

- (7) Tullius, R.; Karimullah, A. S.; Rodier, M.; Fitzpatrick, B.; Gadegaard, N.; Barron, L. D.; Rotello, V. M.; Cooke, G.; Lapthorn, A.; Kadodwala, M. Superchiral" Spectroscopy: Detection of Protein Higher Order Hierarchical Structure with Chiral Plasmonic Nanostructures. *J. Am. Chem. Soc.* **2015**, *137*, 8380–8383.
- (8) Syubaev, S.; Porfirev, A.; Zhizhchenko, A.; Vitrik, O.; Kudryashov, S.; Fomchenkov, S.; Khonina, S.; Kuchmizhak, A. Zero-Orbital-Angular-Momentum Laser Printing of Chiral Nanoneedles. *Opt. Lett.* **2017**, *42*, 5022.
- (9) Fan, J.; Kotov, N. A. Chiral Nanoceramics. *Adv. Mater.* **2020**, *32*, 1906738.
- (10) Yeom, J.; Santos, U. S.; Chekini, M.; Cha, M.; de Moura, A. F.; Kotov, N. A. Chiromagnetic Nanoparticles and Gels. *Science* **2018**, *359*, 309–314.
- (11) Li, Y.; Cheng, J.; Li, J.; Zhu, X.; He, T.; Chen, R.; Tang, Z. Tunable Chiroptical Properties from the Plasmonic Band to Metal-Ligand Charge Transfer Band of Cysteine-Capped Molybdenum Oxide Nanoparticles. *Angew. Chem.* **2018**, *130*, 10393–10397.
- (12) Purcell-Milton, F.; McKenna, R.; Brennan, L. J.; Cullen, C. P.; Guillemeney, L.; Tepliakov, N. V.; Baimuratov, A. S.; Rukhlenko, I. D.; Perova, T. S.; Duesberg, G. S.; Baranov, A. V.; Fedorov, A. V.; Gun'ko, Y. K. Induction of Chirality in Two-Dimensional Nanomaterials: Chiral 2D MoS₂ Nanostructures. *ACS Nano* **2018**, *12*, 954–964.
- (13) Jiang, S.; Chekini, M.; Qu, Z.-B.; Wang, Y.; Yeltik, A.; Liu, Y.; Kotyay, A.; Zhang, T.; Li, B.; Demir, H. V.; Kotov, N. A. Chiral Ceramic Nanoparticles and Peptide Catalysis. *J. Am. Chem. Soc.* **2017**, *139*, 13701–13712.
- (14) Duan, Y.; Han, L.; Zhang, J.; Asahina, S.; Huang, Z.; Shi, L.; Wang, B.; Cao, Y.; Yao, Y.; Ma, L.; Wang, C.; Dukor, R. K.; Sun, L.; Jiang, C.; Tang, Z.; Nafie, L. A.; Che, S. Optically Active Nanostructured ZnO Films. *Angew. Chem., Int. Ed.* **2015**, *54*, 15170–15175.
- (15) Cho, N. H.; Lee, H.; Ahn, H.; Lee, Y. Y.; Im, S. W.; Kim, H.; Nam, K. T. Cysteine Induced Chiral Morphology in Palladium Nanoparticle. *Part. Part. Syst. Charact.* **2019**, *36*, 1900062.
- (16) Han, B.; Zhu, Z.; Li, Z.; Zhang, W.; Tang, Z. Conformation Modulated Optical Activity Enhancement in Chiral Cysteine and Au Nanorod Assemblies. *J. Am. Chem. Soc.* **2014**, *136*, 16104–16107.
- (17) Zhu, Z.; Liu, W.; Li, Z.; Han, B.; Zhou, Y.; Gao, Y.; Tang, Z. Manipulation of Collective Optical Activity in One-Dimensional Plasmonic Assembly. *ACS Nano* **2012**, *6*, 2326–2332.
- (18) Zhu, F.; Li, X.; Li, Y.; Yan, M.; Liu, S. Enantioselective Circular Dichroism Sensing of Cysteine and Glutathione with Gold Nanorods. *Anal. Chem.* **2015**, *87*, 357–361.
- (19) Ben-Moshe, A.; Wolf, S. G.; Sadan, M. B.; Houben, L.; Fan, Z.; Govorov, A. O.; Markovich, G. Enantioselective Control of Lattice and Shape Chirality in Inorganic Nanostructures Using Chiral Biomolecules. *Nat. Commun.* **2014**, *5*, 4302.
- (20) Lu, J.; Chang, Y.-X.; Zhang, N.-N.; Wei, Y.; Li, A.-J.; Tai, J.; Xue, Y.; Wang, Z.-Y.; Yang, Y.; Zhao, L.; Lu, Z.-Y.; Liu, K. Chiral Plasmonic Nanochains via the Self-Assembly of Gold Nanorods and Helical Glutathione Oligomers Facilitated by Cetyltrimethylammonium Bromide Micelles. *ACS Nano* **2017**, *11*, 3463–3475.
- (21) Fu, X.; Wang, Y.; Huang, L.; Sha, Y.; Gui, L.; Lai, L.; Tang, Y. Assemblies of Metal Nanoparticles and Self-Assembled Peptide Fibrils—Formation of Double Helical and Single-Chain Arrays of Metal Nanoparticles. *Adv. Mater.* **2003**, *15*, 902–906.
- (22) Lee, J.; Huh, J.-H.; Kim, K.; Lee, S. DNA Origami-Guided Assembly of the Roundest 60–100 nm Gold Nanospheres into Plasmonic Metamolecules. *Adv. Funct. Mater.* **2018**, *28*, 1707309.
- (23) Kuzyk, A.; Schreiber, R.; Fan, Z.; Pardatscher, G.; Roller, E.-M.; Högele, A.; Simmel, F. C.; Govorov, A. O.; Liedl, T. DNA-Based Self-Assembly of Chiral Plasmonic Nanostructures with Tailored Optical Response. *Nature* **2012**, *483*, 311–314.
- (24) Mastroianni, A. J.; Claridge, S. A.; Alivisatos, A. P. Pyramidal and Chiral Groupings of Gold Nanocrystals Assembled Using DNA Scaffolds. *J. Am. Chem. Soc.* **2009**, *131*, 8455–8459.

- (25) Lee, Y. Y.; Cho, N. H.; Im, S. W.; Lee, H.; Ahn, H.; Nam, K. T. Chiral 432 Helicoid II Nanoparticle Synthesized with Glutathione and Poly(T) 20 Nucleotide. *ChemNanoMat* **2020**, *6*, 362–367.
- (26) Schilthuizen, M.; Davison, A. The Convolved Evolution of Snail Chirality. *Naturwissenschaften* **2005**, *92*, 504–515.
- (27) Schröder-Turk, G. E.; Wickham, S.; Averdunk, H.; Brink, F.; Fitz Gerald, J. D.; Poladian, L.; Large, M. C. J.; Hyde, S. T. The Chiral Structure of Porous Chitin within the Wing-Scales of Callophrys Rubi. *J. Struct. Biol.* **2011**, *174*, 290–295.
- (28) Schaaff, T. G.; Whetten, R. L. Giant Gold-Glutathione Cluster Compounds: Intense Optical Activity in Metal-Based Transitions. *J. Phys. Chem. B* **2002**, *104*, 2630–2641.
- (29) Moloney, M. P.; Gun'ko, Y. K.; Kelly, J. M. Chiral Highly Luminescent CdS Quantum Dots. *Chem. Commun.* **2007**, *7345*, 3900.
- (30) Nakashima, T.; Kobayashi, Y.; Kawai, T. Optical Activity and Chiral Memory of Thiol-Capped CdTe Nanocrystals. *J. Am. Chem. Soc.* **2009**, *131*, 10342–10343.
- (31) Lee, H.-E.; Ahn, H.-Y.; Mun, J.; Lee, Y. Y.; Kim, M.; Cho, N. H.; Chang, K.; Kim, W. S.; Rho, J.; Nam, K. T. Amino-Acid- and Peptide-Directed Synthesis of Chiral Plasmonic Gold Nanoparticles. *Nature* **2018**, *556*, 360–365.
- (32) Lee, H.-E.; Kim, R. M.; Ahn, H.-Y.; Lee, Y. Y.; Byun, G. H.; Im, S. W.; Mun, J.; Rho, J.; Nam, K. T. Cysteine-Encoded Chirality Evolution in Plasmonic Rhombic Dodecahedral Gold Nanoparticles. *Nat. Commun.* **2020**, *11*, 263.
- (33) Kim, H.; Im, S. W.; Cho, N. H.; Seo, D. H.; Kim, R. M.; Lim, Y.; Lee, H.; Ahn, H.; Nam, K. T. Γ -Glutamylcysteine- and Cysteinylglycine-Directed Growth of Chiral Gold Nanoparticles and Their Crystallographic Analysis. *Angew. Chem., Int. Ed.* **2020**, *59*, 12976–12983.
- (34) Ma, W.; Xu, L.; De Moura, A. F.; Wu, X.; Kuang, H.; Xu, C.; Kotov, N. A. Chiral Inorganic Nanostructures. *Chem. Rev.* **2017**, *117*, 8041–8093.
- (35) Im, S. W.; Ahn, H.; Kim, R. M.; Cho, N. H.; Kim, H.; Lim, Y.; Lee, H.; Nam, K. T. Chiral Surface and Geometry of Metal Nanocrystals. *Adv. Mater.* **2020**, *32*, 1905758.
- (36) Kim, H.; Im, S. W.; Kim, R. M.; Cho, N. H.; Lee, H.-E.; Ahn, H.-Y.; Nam, K. T. Chirality Control of Inorganic Materials and Metals by Peptides or Amino Acids. *Mater. Adv.* **2020**, *1*, 512–524.
- (37) Lee, J.; Choe, I. R.; Kim, Y.-O.; Namgung, S. D.; Jin, K.; Ahn, H.-Y.; Sung, T.; Kwon, J.-Y.; Lee, Y.-S.; Nam, K. T. Proton Conduction in a Tyrosine-Rich Peptide/Manganese Oxide Hybrid Nanofilm. *Adv. Funct. Mater.* **2017**, *27*, 1702185.
- (38) Lee, J.; Ju, M.; Cho, O. H.; Kim, Y.; Nam, K. T. Tyrosine-Rich Peptides as a Platform for Assembly and Material Synthesis. *Adv. Sci.* **2019**, *6*, 1801255.
- (39) Cherny, I.; Gazit, E. Amyloids: Not Only Pathological Agents but Also Ordered Nanomaterials. *Angew. Chem., Int. Ed.* **2008**, *47*, 4062–4069.
- (40) Wei, G.; Su, Z.; Reynolds, N. P.; Arosio, P.; Hamley, I. W.; Gazit, E.; Mezzenga, R. Self-Assembling Peptide and Protein Amyloids: From Structure to Tailored Function in Nanotechnology. *Chem. Soc. Rev.* **2017**, *46*, 4661–4708.
- (41) Hamill, S. J.; Cota, E.; Chothia, C.; Clarke, J. Conservation of Folding and Stability within a Protein Family: The Tyrosine Corner as an Evolutionary Cul-de-Sac 1 Edited by J. M. Thornton. *J. Mol. Biol.* **2000**, *295*, 641–649.
- (42) McConnell, I.; Li, G.; Brudvig, G. W. Energy Conversion in Natural and Artificial Photosynthesis. *Chem. Biol.* **2010**, *17*, 434–447.
- (43) Sevier, C. S.; Kaiser, C. A. Formation and Transfer of Disulphide Bonds in Living Cells. *Nat. Rev. Mol. Cell Biol.* **2002**, *3*, 836–847.
- (44) Jang, H.-S.; Lee, J.-H.; Park, Y.-S.; Kim, Y.-O.; Park, J.; Yang, T.-Y.; Jin, K.; Lee, J.; Park, S.; You, J. M.; Jeong, K.-W.; Shin, A.; Oh, I.-S.; Kwon, M.-K.; Kim, Y.-I.; Cho, H.-H.; Han, H. N.; Kim, Y.; Chang, Y. H.; Paik, S. R.; et al. Tyrosine-Mediated Two-Dimensional Peptide Assembly and Its Role as a Bio-Inspired Catalytic Scaffold. *Nat. Commun.* **2014**, *5*, 3665.
- (45) Gu, F.; Li, C.; Hu, Y.; Zhang, L. Synthesis and Optical Characterization of Co₃O₄ Nanocrystals. *J. Cryst. Growth* **2007**, *304*, 369–373.
- (46) Lenglet, M.; Jørgensen, C. K. Reinvestigation of the Optical Properties of Co₃O₄. *Chem. Phys. Lett.* **1994**, *229*, 616–620.
- (47) Engel, J.; Liehl, E.; Sorg, C. Circular Dichroism, Optical Rotatory Dispersion and Helix Coil Transition of Polytyrosine and Tyrosine Peptides in Non-Aqueous Solvents. *Eur. J. Biochem.* **1971**, *21*, 22–30.
- (48) Antosiewicz, J. M.; Shugar, D. UV-Vis Spectroscopy of Tyrosine Side-Groups in Studies of Protein Structure. Part 1: Basic Principles and Properties of Tyrosine Chromophore. *Biophys. Rev.* **2016**, *8*, 151–161.
- (49) Alrehaily, L. M.; Joseph, J. M.; Biesinger, M. C.; Guzonas, D. A.; Wren, J. C. Gamma-Radiolysis-Assisted Cobalt Oxide Nanoparticle Formation. *Phys. Chem. Chem. Phys.* **2013**, *15*, 1014–1024.
- (50) Sivo, V.; D'Abrasca, G.; Russo, L.; Iacovino, R.; Pedone, P. V.; Fattorusso, R.; Isernia, C.; Malgieri, G. Co(II) Coordination in Prokaryotic Zinc Finger Domains as Revealed by UV-Vis Spectroscopy. *Bioinorg. Chem. Appl.* **2017**, *2017*, 1–7.
- (51) May, S. W.; Kuo, J.-Y. Preparation and Properties of Cobalt (II) Rubredoxin. *Biochemistry* **1978**, *17*, 3333–3338.
- (52) Nitsche, C.; Otting, G. Pseudocontact Shifts in Biomolecular NMR Using Paramagnetic Metal Tags. *Prog. Nucl. Magn. Reson. Spectrosc.* **2017**, *98–99*, 20–49.
- (53) Lovell, S. C.; Davis, I. W.; Arendall, W. B.; de Bakker, P. I. W.; Word, J. M.; Prisant, M. G.; Richardson, J. S.; Richardson, D. C. Structure Validation by $\text{C}\alpha$ Geometry: ϕ, ψ and $\text{C}\beta$ Deviation. *Proteins: Struct., Funct., Genet.* **2003**, *50*, 437–450.
- (54) Cavins, J. F.; Krull, L. H.; Friedman, M.; Gibbs, D. E.; Inglett, G. E. Spectrophotometric Cysteine Analysis. *J. Agric. Food Chem.* **1972**, *20*, 1124–1126.
- (55) Han, B.; Gao, X.; Lv, J.; Tang, Z. Magnetic Circular Dichroism in Nanomaterials: New Opportunity in Understanding and Modulation of Excitonic and Plasmonic Resonances. *Adv. Mater.* **2020**, *32*, 1801491.
- (56) Eslami, S.; Gibbs, J. G.; Reckkemmer, Y.; van Slageren, J.; Alarcón-Correa, M.; Lee, T.-C.; Mark, A. G.; Rikken, G. L. J. A.; Fischer, P. Chiral Nanomagnets. *ACS Photonics* **2014**, *1*, 1231–1236.
- (57) Werth, M. T.; Tang, S. F.; Formicka, G.; Zeppezauer, M.; Johnson, M. K. Magnetic Circular Dichroism and Electron Paramagnetic Resonance Studies of Cobalt-Substituted Horse Liver Alcohol Dehydrogenase. *Inorg. Chem.* **1995**, *34*, 218–228.
- (58) Bergman, T.; Jornvall, H.; Holmquist, B.; Vallee, B. L. A Synthetic Peptide Encompassing the Binding Site of the Second Zinc Atom (the “Structural” Zinc) of Alcohol Dehydrogenase. *Eur. J. Biochem.* **1992**, *205*, 467–470.
- (59) Xu, H.; Zeng, H. C. Self-Generation of Tiered Surfactant Superstructures for One-Pot Synthesis of Co 3O 4 Nanocubes and Their Close-and Non-Close-Packed Organizations. *Langmuir* **2004**, *20*, 9780–9790.
- (60) George, G.; Anandhan, S. A Comparative Study on the Physico-Chemical Properties of Sol-Gel Electrospun Cobalt Oxide Nanofibres from Two Different Polymeric Binders. *RSC Adv.* **2015**, *5*, 81429–81437.
- (61) Lee, W.; Tonelli, M.; Markley, J. L. NMRFAM-SPARKY: Enhanced Software for Biomolecular NMR Spectroscopy. *Bioinformatics* **2015**, *31*, 1325–1327.
- (62) Herrmann, T.; Güntert, P.; Wüthrich, K. Protein NMR Structure Determination with Automated NOE Assignment Using the New Software CANDID and the Torsion Angle Dynamics Algorithm DYANA. *J. Mol. Biol.* **2002**, *319*, 209–227.